PAPER

Development of variational guiding center algorithms for parallel calculations in experimental magnetic equilibria

To cite this article: C Leland Ellison *et al* 2015 *Plasma Phys. Control. Fusion* **57** 054007

IOP Publishing Plasma Physics and Controlled Fusion
Plasma Phys. Control. Fusion **57** (2015) 054007 (13pp) doi:10.1088/0741-3335/57/5/054007

Development of variational guiding center algorithms for parallel calculations in experimental magnetic equilibria

C Leland Ellison[1], J M Finn[2], H Qin[1,3] and W M Tang[1]

[1] Princeton Plasma Physics Laboratory, Princeton, NJ, 08550 USA
[2] Los Alamos National Laboratory, Los Alamos, NM 87545, USA
[3] Department of Modern Physics, University of Science and Technology of China, Hefei, Anhui 230026, People's Republic of China

E-mail: lellison@pppl.gov

Received 17 October 2014, revised 2 January 2015
Accepted for publication 15 January 2015
Published 15 April 2015

Abstract

Structure-preserving algorithms obtained via discrete variational principles exhibit strong promise for the calculation of guiding center test particle trajectories. The non-canonical Hamiltonian structure of the guiding center equations forms a novel and challenging context for geometric integration. To demonstrate the practical relevance of these methods, a prototypical variational midpoint algorithm is applied to an experimental magnetic equilibrium. The stability characteristics, conservation properties and implementation requirements associated with the variational algorithms are addressed. Furthermore, computational run time is reduced for large numbers of particles by parallelizing the calculation to use general-purpose graphics processing unit hardware.

Keywords: guiding center algorithms, parallel calculations, magnetic equilibria, variational integrators

(Some figures may appear in colour only in the online journal)

1. Introduction

One of the principle challenges of plasma physics is to accurately model multi-scale phenomena. As magnetically confined fusion plasmas progress toward the burning plasma regime, the largest characteristic temporal and spatial scales grow increasingly disparate from the smallest. For instance, the gyro-orbits exhibited by electrons in ITER will occur at a timescale thirteen orders of magnitude faster than the pulse discharge length. Numerically modeling test particle dynamics in burning plasma devices thus presents a formidable challenge. The analytic guiding center transformation partially mitigates this challenge by shifting the shortest characteristic timescale from the gyroperiod to the toroidal transit time. However, modeling the dynamics of fast particles such as runaway electrons and hot alphas still requires resolving tens of thousands of toroidal transits. The numerical computation of such long term dynamics stands to benefit from advances in algorithms and computational hardware.

On the numerical analysis front, so-called 'geometric' algorithms retain physically conserved quantities in the numerically simulated dynamics, resulting in excellent long term numerical fidelity [1]. An algorithm that conserves energy or momentum more accurately represents the physical system after many numerical time advances than an algorithm that conserves no such quantities. In essence, while truncation error is unavoidable in any numerical approximation, numerically conserved quantities force the errors to manifest in relatively benign features, such as in the phase of a periodic trajectory. The importance of magnetically confined fast particle dynamics makes the calculation of guiding center trajectories an appealing candidate for application of structure preserving algorithms.

Moreover, the guiding center equations of motion are an especially novel context for geometric integration because the most natural description of the dynamics is non-canonically Hamiltonian [2, 3]. A popular class of geometric algorithms for Hamiltonian systems preserves a 'symplectic structure'

used in the formulation of the Hamiltonian system. From a geometric perspective, the content of Hamilton's equations is independent of the coordinates used to represent them [4, 5]. However, nearly all symplectic algorithms rely on representing Hamilton's equations in coordinates exhibiting the canonical position-**q**, conjugate momentum-**p** pairing [1]. The task of developing numerical methods that preserve the symplectic structure of non-canonical Hamilton's equations remains an outstanding challenge in the field of numerical analysis [1, 6]. While the guiding center equations of motion may be cast in canonical coordinates [3, 7, 8], a global transformation may not exist for arbitrary magnetic geometry and local transformations may be undesirably complex for magnetic configurations of interest [9].

One technique for constructing algorithms ensures the presence of conserved quantities by discretizing the variational principle that underlies the equations of motion [10]. By requiring the discrete trajectory to extremize a discrete action, the numerical time advance inherits several conservation properties of the continuous dynamics. Such an approach has proven insightful for the analysis of familiar symplectic algorithms [10] while yielding novel schemes unlikely to arise from direct discretization of the equations of motion [11–13]. The success of variational algorithms motivated studies in discretizing the guiding center Lagrangian, yielding test cases in simple magnetic geometry that exhibited the characteristic long-term numerical fidelity [14–18]. As will be detailed in this paper, the conservation properties of variational guiding center algorithms require more nuanced interpretation than those of the conventional variational integrators.

In this article, variational algorithms are discussed as high-performance methods for guiding center test particle calculations that leverage advances in conservative numerical methods and parallel computing hardware. Background is first presented to establish that variational integration in the guiding center context is a foray into the little-explored realms of degenerate Lagrangians and geometric integration of non-canonical Hamiltonian systems. We then explain unique challenges that emerge as a result of employing variational integrators in this atypical setting. In particular, the multistep characteristics of the guiding center variational algorithms require careful interpretation of the stability and conservation properties. A specific and unobvious initialization procedure is described for minimizing the amplitudes of the non-physical component of the numerical dynamics. Addressing these issues was necessary for expanding upon the early positive results to obtain good long-term numerical fidelity in more complicated and realistic magnetic geometry. We discuss implementation details of interfacing the guiding center algorithm with the EFIT equilibrium code and provide numerical benchmarks against non-geometric algorithms. To expand the practical relevance of this family of algorithms, run time reduction is achieved for large numbers of test particles by implementing the variational algorithms on general-purpose graphics processing units (GPGPUs) using the CUDA programming language. Overall, the observed long-term numerical fidelity in experimentally-relevant configurations and ability to highly parallelize the calculation illustrate the promise of variational methods for performing high-performance guiding center test particle calculations.

2. Background

To establish context for the variational guiding center algorithms, this section reviews guiding center dynamics and variational integration. In discussing the guiding center system, emphasis is placed on understanding the equations of motion as a Hamiltonian system described by non-canonical coordinates. Variational integrators are then presented as a systematic means of deriving symplectic algorithms for the time advance of Hamiltonian systems described by canonical coordinates. This sets the stage for future sections to describe extensions of the variational integrator methodology to model the non-canonical guiding center system.

2.1. Hamiltonian guiding center dynamics

A prominent technique for reducing the complexity of magnetized charged particle dynamics is the transformation to guiding center coordinates [2, 3]. If the scale length over which the electric and magnetic fields vary is much longer than the radius at which a charged particle orbits a magnetic field line, the dynamics are approximately invariant with respect to the phase of the particle's gyro-orbit. Analytically, transforming to coordinates in which this invariance is manifest reduces the dimensionality of the dynamics from six dimensions to four. Numerically, one no longer needs to resolve the rapid gyromotion while tracking the guiding center of the particle orbit along and across magnetic field lines.

Beginning from the standard Lorentz force description of a charged particle in electric and magnetic fields, the guiding center transformation is an approximate transformation from the original charged particle position $\mathbf{q}$ and velocity $\mathbf{v}$ to the position of the guiding center $\mathbf{x}$ and three additional variables (u, μ, Θ). Here, u is the velocity of the guiding center along the magnetic field line, μ is the magnetic moment and Θ is the gyrophase, which is the angle of the gyro-orbit with respect to some initial position. In the new coordinates, the (Θ, μ) dynamics decouple from the other components and may be ignored if only the guiding center position and velocity are of interest. To determine the equations of motion in the guiding center coordinates $(\mathbf{x}, u, \mu, \Theta)$, one refers to the foundational frameworks for deriving charged particle equations of motion: the Lagrangian and Hamiltonian formalisms.

From the Lagrangian perspective, one may derive the familiar Lorentz force law starting from the charged particle Lagrangian:

$$L(\mathbf{q}, \dot{\mathbf{q}}) = \frac{1}{2} m \mid \dot{\mathbf{q}} \mid^2 + \frac{e}{c} \mathbf{A} \cdot \dot{\mathbf{q}} - e\phi \,. \tag{1}$$

Here, $\dot{\mathbf{q}} = \dfrac{\mathrm{d}\mathbf{q}}{\mathrm{d}t}$, m is the mass of the particle, e is the charge, $\mathbf{A}$ is the vector potential and ϕ is the scalar potential, both assumed to be time-independent for simplicity. For the purposes of this discussion, we deem this Lagrangian a 'configuration-space

Lagrangian', as it acts on points $(\mathbf{q}, \dot{\mathbf{q}})$ in the tangent bundle TQ of the configuration space Q [4]. Next, one defines an action functional S acting on paths that traverse the configuration space as parameterized by a time coordinate t. Given a twice-differentiable path $\mathbf{q}(t)$ with endpoints $t = 0$, $t = T$, the action functional S is defined by:

$$S(\mathbf{q}) = \int_0^T L(\mathbf{q}(t), \dot{\mathbf{q}}(t))\mathrm{d}t. \tag{2}$$

Requiring the action to be extremized with respect to arbitrary path variations $\delta\mathbf{q}$ with fixed endpoints $(\delta\mathbf{q}(t = 0) = \delta\mathbf{q}(t = T) = 0)$, one finds the Euler–Lagrange equations for a charged particle:

$$m\ddot{\mathbf{q}} = e\mathbf{E} + \frac{e}{c}\dot{\mathbf{q}} \times \mathbf{B}\,. \tag{3}$$

Here we see the electric field $\mathbf{E} = -\nabla\phi$ and the magnetic field $\mathbf{B} = \nabla \times \mathbf{A}$.

Instead of a second-order differential equation in three variables, one may describe the dynamics as a system first-order equations in six variables by turning to the Hamiltonian perspective. The Hamiltonian for a charged particle is given by:

$$H(\mathbf{q},\ \mathbf{p}) = \frac{1}{2m}|\mathbf{p} - \frac{e}{c}\mathbf{A}|^2 + \ e\phi, \tag{4}$$

where the momentum $\mathbf{p} = m\dot{\mathbf{q}} + \frac{e}{c}\mathbf{A}$. The equations of motion are given by Hamilton's canonical equations:

$$\dot{\mathbf{q}} = \frac{\partial H}{\partial \mathbf{p}} \qquad \dot{\mathbf{p}} = -\frac{\partial H}{\partial \mathbf{q}}\,. \tag{5}$$

These two formulations offer equivalent descriptions of the dynamics while exhibiting different flexibility in their potential for coordinate transformations. From the Lagrangian perspective, one is free to transform the three configuration coordinates q^i $(i = 1, 2, 3)$; extremizing the action with respect to perturbations in the new coordinates recovers the proper dynamics. However, the velocity variables $\dot{q}^i$ are directly determined as the time derivatives of the configuration coordinates, thereby restricting the ability to transform the velocity coordinates. Alternatively, the Hamiltonian description elevates the momenta $\mathbf{p}$ to equal status as the configuration coordinates $\mathbf{q}$. The restriction in this setting is that transformations performed on the six variables $(\mathbf{q}, \mathbf{p})$ to new coordinates $(z^1, ..., z^6)$ must retain the canonical coordinate pairing in the new variables. Otherwise, one must consider how the Poisson bracket transforms, which is a less straightforward task than the variational principle utilized in the Lagrangian context. Neither of these two formalisms offers the desired freedom of transforming from physical charged particle coordinates $(\mathbf{q}, \mathbf{v})$ to the guiding center coordinates $(\mathbf{x}, u, \mu, \Theta)$.

A hybrid approach facilitates the calculation of Hamiltonian equations in general coordinates by utilizing an action principle in phase space [5, 19]. Given phase-space coordinates $(\mathbf{q}, \mathbf{p})$, consider the 'phase-space Lagrangian' given by:

$$L(\mathbf{q}, \mathbf{p}, \dot{\mathbf{q}}, \dot{\mathbf{p}}) = \mathbf{p} \cdot \dot{\mathbf{q}} - H(\mathbf{q}, \mathbf{p}). \tag{6}$$

This expression for the Lagrangian is numerically equivalent to that given by the Legendre transform, but here $\mathbf{q}$ and $\mathbf{p}$ are retained as independent coordinates. The critical distinction with the configuration-space Lagrangian is that the linear dependence on the velocities $(\dot{\mathbf{p}}, \dot{\mathbf{q}})$ results in a *first*-order differential equation upon application of the variational principle. Because the Euler–Lagrange equations are not second-order, the phase-space Lagrangian is said to be 'degenerate'. Extremizing the action integral of the phase-space Lagrangian with respect to arbitrary fixed-endpoint path variations $(\delta\mathbf{q}, \delta\mathbf{p})$ recovers equation (5) as the 'Euler–Lagrange equations'. By deriving Hamilton's equations from a variational principle, arbitrary transformation of the six phase-space coordinates may be performed and determination of the equations of motion in the new coordinates simply requires extremizing the action with respect to paths represented by the new coordinates.

This phase-space Lagrangian is the starting point for the transformation to guiding center coordinates. One manipulates the charged particle phase-space Lagrangian, neglecting small terms in the mass-to-charge ratio. The resulting guiding center Lagrangian is given by:

$$\begin{aligned} &L(\mathbf{x}, u, \mu, \Theta, \dot{\mathbf{x}}, \dot{u}, \dot{\mu}, \dot{\Theta}) \\ &= \left(\frac{e}{mc}\mathbf{A} + u\mathbf{b}\right) \cdot \dot{\mathbf{x}} + \frac{c}{e}\mu\dot{\Theta} - \left(\frac{u^2}{2} + \mu B + \frac{e}{m}\phi\right), \end{aligned} \tag{7}$$

where $\mathbf{b}$ is the magnetic field unit vector and B the magnetic field magnitude. We emphasize that this Lagrangian originates from equation (6), not the charged particle Lagrangian equation (1). In resemblance to the canonical phase-space Lagrangian of equation (6), the guiding center Lagrangian is linear in the velocities $(\dot{\mathbf{x}}, \dot{u}, \dot{\mu}, \dot{\theta})$ and includes the guiding center Hamiltonian:

$$H_{\mathrm{gc}}(\mathbf{x}, u, \mu, \Theta) = \frac{u^2}{2} + \mu B + \frac{e}{m}\phi\,. \tag{8}$$

The action of the guiding center Lagrangian is extremized with respect to variations $(\delta\,\mathbf{x}, \delta u, \delta\,\mu, \delta\,\Theta)$ by paths satisfying the following first-order ODE system:

$$\begin{aligned} (A^{\dagger}_{i,j} - A^{\dagger}_{j,i})\dot{x}^i - \dot{u}b_j - \left(\mu B_{,j} + \frac{e}{m}\phi_{,j}\right) &= 0 \qquad j = 1, 2, 3 \\ b_i\dot{x}^i - u &= 0 \\ \dot{\mu} &= 0 \\ \dot{\Theta} - \frac{eB}{mc} &= 0 \end{aligned} \tag{9}$$

Here, $\mathbf{A}^{\dagger} = \frac{e}{mc}\mathbf{A} + u\mathbf{b}$, summation over repeated indices is implied and indices appearing after a comma denote differentiation with respect to the corresponding component. As desired from the onset of the guiding center transformation, the (μ, Θ) dynamics decouple from the $(\mathbf{x}, u)$ dynamics. Henceforth, μ will be treated as constant and the gyrophase Θ ignored.

Upon inspection of the guiding center equation (9), it is clear the ODE system does not have the canonical Hamiltonian form of equation (5). Indeed, they were obtained via an action principle in phase space following a non-canonical coordinate

transformation. While equation (5) are the familiar setting for discussing Hamiltonian dynamics, the guiding center equations are encapsulated by a more general notion of Hamiltonian systems of the form:

$$\Omega_{ij}\dot{z}^i = H_{,j} \qquad j = 1, \ldots, 2n, \tag{10}$$

where Ω is a non-degenerate anti-symmetric matrix and $2n$ is the dimension of the Hamiltonian phase space (see e.g. equation (5.4.1) of [5]). The canonical case of equation (5) may be viewed as a specific instance of equation (10) in which $\mathbf{z} = (\mathbf{q}, \mathbf{p})$ and $\Omega = \begin{bmatrix} 0 & I \\ -I & 0 \end{bmatrix}$. The guiding center equations are also in the form of equation (10) with $\mathbf{z} = (\mathbf{x}, u)$ and

$$\Omega = \begin{bmatrix} 0 & -B_3^\dagger & B_2^\dagger & b_1 \\ B_3^\dagger & 0 & -B_1^\dagger & b_2 \\ -B_2^\dagger & B_1^\dagger & 0 & b_3 \\ -b_1 & -b_2 & -b_3 & 0 \end{bmatrix}, \tag{11}$$

where $\mathbf{B}^\dagger = \nabla \times \mathbf{A}^\dagger$. It is in this sense that the four-dimensional guiding center equations are considered non-canonically Hamiltonian.

The anti-symmetric matrix Ω appearing in equation (10) plays a prominent role in the conservation properties of Hamiltonian systems: it is known as the 'symplectic structure' and relates to the preservation of phase-space area. Solutions to Hamilton's equations are said to preserve the symplectic structure or simply to 'be symplectic'. The terminology refers to preserving the symplectic structure Ω, however, simply evaluating the components of the matrix in equation (11) along different points of the trajectory of a guiding center test particle, for instance, will *not* yield equivalent results. The correct interpretation considers how the symplectic structure acts on pairs of vectors located at different positions in the Hamiltonian phase space. Suppose some initial position in the Hamiltonian phase space $\mathbf{z}$ and two vectors $\mathbf{u}$, $\mathbf{v}$ located at the position $\mathbf{z}$—these are called tangent vectors. The symplectic structure Ω may be used to calculate a real number corresponding to this pair of tangent vectors according to $\Omega(\mathbf{u}, \mathbf{v}) = \Omega_{ij} u^i v^j$, where the components of Ω are evaluated at the position $\mathbf{z}$. Next, suppose we advance $\mathbf{z}$ to a new position in phase space $\mathbf{Z}$ according to some map Φ. That is, $\Phi(\mathbf{z}) = \mathbf{Z}$. The tangent vectors $(\mathbf{u}, \mathbf{v})$ may also be advanced to new vectors $(\mathbf{U}, \mathbf{V})$ at $\mathbf{Z}$ according to the calculus chain rule: $U^i = \Phi^i_{\ j} u^j$ and similarly for $\mathbf{V}$ from $\mathbf{v}$. The map Φ is said to be symplectic with respect to Ω if $\Omega(\mathbf{U}, \mathbf{V}) = \Omega(\mathbf{u}, \mathbf{v})$ for arbitrary $(\mathbf{u}, \mathbf{v})$, where the Ω on the left hand side is evaluated at $\mathbf{Z}$ and the Ω on the right hand size is evaluated at $\mathbf{z}$. Because this must be true for arbitrary pairs of tangent vectors $(\mathbf{u}, \mathbf{v})$, satisfaction of the symplecticity condition only depends on Φ, its Jacobian matrix of derivatives $D\Phi$ and Ω. This somewhat nuanced relationship between Φ and Ω may be concisely represented using the pull-back notation from differential geometry [5]:

$$\Phi^*\Omega = D\Phi^T\, \Omega\, D\Phi = \Omega\,. \tag{12}$$

It can be shown directly from the action principle in phase space that solutions to equation (10) have this property of being symplectic. In the case that the symplectic structure is the canonical structure $\Omega = \begin{bmatrix} 0 & I \\ -I & 0 \end{bmatrix}$, the symplecticity requirement is equivalent to preserving phase-space area.

Many important theorems about Hamiltonian dynamics leverage the fact that solutions to Hamilton's equations are symplectic. The explanation of symplecticity is thus important for understanding a major implication of the Hamiltonian formulation of guiding center dynamics and for discussing an important class of conservative numerical methods adapted to the study of Hamiltonian systems: symplectic integrators.

2.2. Variational integration

Symplectic integrators are well-suited for modeling the long-term behavior of Hamiltonian systems because the trajectories they generate exactly sample *some* Hamiltonian system nearby to the original [1]. By virtue of the numerical time advance preserving the same symplectic structure as the true solution to Hamilton's equations, the numerical trajectory may be understood as a discrete sampling of a Hamiltonian system that converges to the original as the numerical step size tends to zero. Conventionally, symplectic integrators are obtained by directly discretizing Hamilton's equations in canonical coordinates and checking the symplecticity condition of equation (12). A more systematic approach to deriving symplectic algorithms is advantageous and has been developed by the theory of variational integrators. Just as a complimentary description of the continuous Hamiltonian dynamics resides in the Lagrangian formalism, symplectic integrators may be understood as resultant from discrete variational principles. Instead of discretizing Hamilton's equations, one may discretize the variational principle used in Lagrangian mechanics and the resulting numerical time-advance maps are guaranteed to be symplectic [5].

Suppose, for instance, a configuration space Lagrangian $L(\mathbf{q}, \dot{\mathbf{q}})$ with action given by equation (2) and Euler–Lagrange equations:

$$\frac{\partial L}{\partial \mathbf{q}} - \frac{\mathrm{d}}{\mathrm{d}t}\frac{\partial L}{\partial \dot{\mathbf{q}}} = 0. \tag{13}$$

If the Lagrangian is regular, i.e. the Hessian matrix $\dfrac{\partial^2 L}{\partial \dot{\mathbf{q}}^2}$ is non-degenerate, then the Euler–Lagrange equations constitute a second-order ODE system and a unique path $\mathbf{q}(t)$ extremizes the action integral, assuming the endpoints are sufficiently close together. The action principle may be discretized by first defining a discrete Lagrangian function L_d that approximates a small interval of the action:

$$L_d(\mathbf{q}_k, \mathbf{q}_{k+1}) \approx \int_{t_k}^{t_{k+1}} L(\mathbf{q}(t), \dot{\mathbf{q}}(t))\mathrm{d}t, \tag{14}$$

where $\mathbf{q}(t)$ in the integrand is the unique trajectory satisfying equation (13) with endpoints (t_k, t_{k+1}) and $\mathbf{q}_k$, $\mathbf{q}_{k+1}$ on the left hand side are the numerical approximations of the solution at times t_k and t_{k+1}, respectively. A discrete action corresponding to a particular choice of discrete Lagrangian is identified as:

$$S_d(\mathbf{q}_0, \ldots, \mathbf{q}_N) = \sum_{k=0}^{N-1} L_d(\mathbf{q}_k, \mathbf{q}_{k+1}), \tag{15}$$

where $\mathbf{q}_0 = \mathbf{q}(t = 0)$ is the initial condition and $t_N = T$ is the end point. Variation of the action with respect to $\delta\,\mathbf{q}_k$ for arbitrary $k \in \{1, ..., N-1\}$ yields the 'discrete Euler–Lagrange equations':

$$D_2L_d(\mathbf{q}_{k-1}, \mathbf{q}_k) + D_1L_d(\mathbf{q}_k, \mathbf{q}_{k+1}) = 0, \tag{16}$$

where the slot derivative D_i denotes differentiation with respect to the i-th argument. The discrete Euler–Lagrange equation (16) is a numerical method for approximating the solution of the continuous Euler–Lagrange equation (13). Simple choices for the discrete Lagrangian can yield familiar algorithms, such as the Störmer–Verlet method [10].

The variationally derived discrete Euler–Lagrange equations may be formulated as a canonically symplectic map for the solution of Hamilton's equation (5). The identification of a symplectic map follows from defining a 'discrete Legendre transform':

$$\begin{aligned} \mathbf{p}_k &= -D_1L_d(\mathbf{q}_k, \mathbf{q}_{k+1}) \\ \mathbf{p}_{k+1} &= D_2L_d(\mathbf{q}_k, \mathbf{q}_{k+1}). \end{aligned} \tag{17}$$

These seemingly different definitions for the discrete momenta are equivalent for numerical trajectories satisfying the discrete Euler–Lagrange equation (16). One may thus iterate equation (17) as a numerical integrator for Hamilton's equations; symplecticity of the algorithm is a consequence of the discrete action principle [10]. Inspection of equation (16) identifies the discrete Lagrangian L_d as a type-one generating function for the canonical transformation $(\mathbf{p}_k, \mathbf{q}_k)$ to $(\mathbf{p}_{k+1}, \mathbf{q}_{k+1})$, guaranteeing the numerical time advance will be symplectic.

The theory of variational integrators forms an elegant discrete analogue to the continuous theory of Lagrangian and Hamiltonian mechanics. In the context of geometric integration of guiding center trajectories, the assumption of the regularity of the Lagrangian complicates the analogy between the continuous and the discrete variational systems. Conventionally, the Euler–Lagrange equations are second order and a Legendre transform is used to relate the Euler–Lagrange equations to a Hamiltonian system and to identify a symplectic algorithm that is equivalent to the variational integrator. For the degenerate phase-space Lagrangians, the Hamiltonian system and the Euler–Lagrange equations are one and the same. The implications of this degeneracy for variationally-derived algorithms will be explored in detail in the following section.

3. Variational guiding center algorithms

We turn now to the task of integrating the guiding center equations of motion equation (9) in a structure-preserving manner. Inspired by the success of discretizing configuration-space action principles, recent work developed guiding center algorithms by discretizing the guiding center Lagrangian [14–18]. Two-dimensional test problems demonstrated excellent long-term numerical fidelity [14–16]. In the process of extending these results to more complicated magnetic geometry, several issues appeared as a consequence of the degeneracy of the guiding center Lagrangian. These complications originate from the fact that the variational guiding center algorithms are multistep methods for the integration of first-order differential equations. Successful use of multistep methods requires mitigating a class of instabilities known as parasitic modes [1, 20]. In section 3.2.1, we derive the presence of these modes for guiding center variational integrators. A mitigation method is proposed in section 3.2.2 by adapting the backward error analysis of [1, 20] to generate smooth initial conditions for the variational guiding center algorithms. To reconcile the presence of these instabilities with the conservation properties of the variational algorithms, an analysis is presented in section 3.2.3 to identify what is preserved by the multistep variational algorithms. A final implementation requirement particular to variational guiding center algorithms is the necessity of evaluating the magnetic vector potential in the numerical update rule and our method of doing so for the EFIT equilibrium code is described in section 3.3.

3.1. Midpoint discretization

The variational integrators literature offers many candidate discretization schemes for application to the guiding center Lagrangian [10–13]. As a representative example, we will primarily consider a non-relativistic version of the midpoint discrete Lagrangian described in [16]:

$$\begin{aligned} L_d(\mathbf{x}_k, u_{k+1/2}, \mathbf{x}_{k+1}) = {} & A_i^\dagger\left(\frac{\mathbf{x}_k + \mathbf{x}_{k+1}}{2}, u_{k+1/2}\right)(x^i_{k+1} - x^i_k) \\ & - hH_{\mathrm{gc}}\left(\frac{\mathbf{x}_k + \mathbf{x}_{k+1}}{2}, u_{k+1/2}\right), \end{aligned} \tag{18}$$

where H_{gc} is given by equation (8). The centered position evaluations are expected to yield a second-order accurate algorithm and the absence of $\dot{u}$ in the guiding center Lagrangian allows staggering the u coordinate at half-integer times.

The discrete Euler–Lagrange equations corresponding to the midpoint discrete Lagrangian are given by:

$$\begin{aligned} &\frac{1}{2}A^\dagger_{i,j}(k+1/2)[x^i_{k+1} - x^i_k] + \frac{1}{2}A^\dagger_{i,j}(k-1/2)[x^i_k - x^i_{k-1}] \\ &\quad - \left[A^\dagger_j(k+1/2) - A^\dagger_j(k-1/2)\right] \\ &\quad - \frac{h}{2}[\mu B_{,j}(k+1/2) + \mu B_{,j}(k-1/2) \\ &\quad + \phi_j(k+1/2) + \phi_j(k-1/2)] = 0, \quad j = 1, 2, 3 \\ &\quad b_i(k+1/2)[x^i_{k+1} - x^i_k] - hu_{k+1/2} = 0. \end{aligned} \tag{19}$$

Here, factors of e and m have been normalized into the definitions of the fields and $(k + 1/2)$ in the function evaluations indicates evaluation at $\left(\mathbf{x} = \frac{\mathbf{x}_k + \mathbf{x}_{k+1}}{2}, u = u_{k+1/2}\right)$ and $(k - 1/2)$ is one time index earlier. These equations resemble the non-canonically Hamiltonian guiding center equations of motion written in the form of equation (10).

The variational guiding center algorithm equation (19) exhibits three features of interest: it is implicit, it is multistep

and the vector potential is evaluated. As an implicit algorithm, implementation involves performing a nonlinear solve. In practice, Newton–Rhapson iterations typically converge within two to three iterations. One might strive for a discretization yielding an explicit variational algorithm, but the work of [17] demonstrated that all explicit variational guiding center algorithms within a natural family of discrete Lagrangians were unstable. By multistep, we mean that equation (19) depends on the previous two positions in time ($\mathbf{x}_{k-1}$, $\mathbf{x}_k$) to determine the new position ($\mathbf{x}_{k+1}$). This may be expected from the form of the discrete Euler–Lagrange equation (16), but is novel for integrating a first-order system of differential equations. Finally, the presence of the magnetic vector potential **A** will require constructing a vector potential from experimental equilibria specified in terms of the magnetic field **B**.

3.2. Multistep characteristics

Multistep numerical methods possess several drawbacks in the context of structure-preserving algorithms that must be addressed and mitigated to successfully utilize the variational guiding center algorithms. From a stability perspective, multistep methods are well-known to exhibit unphysical oscillations known as 'parasitic modes' [1, 20, 21]. These modes must remain small for the temporal simulation domain of interest. A related issue is that *linear* multistep methods cannot be symplectic in the conventional sense [22] and although equation (19) is not a linear multistep method, it would be a surprising feature if it were symplectic in the sense of equation (12). This subsection endeavors to explain (and improve) the behavior of variational guiding center algorithms by investigating the presence of parasitic modes and analyzing conserved quantities of the multistep algorithm.

3.2.1. Parasitic modes. Multistep numerical algorithms admit parasitic modes, which are unphysical artifacts arising from the numerical dynamics occurring in a larger-dimensional space than that of the physical dynamics. Whereas the exact solution to the guiding center equations is uniquely determined by a single initial condition ($\mathbf{x}_0$, u_0), iteration of the variational guiding center algorithm requires two initial conditions. This additional freedom allows unphysical even-odd oscillations to be present in the numerical trajectory. Ensuring the parasitic modes are smaller than the principle behavior is therefore important for successful application of the multistep variational algorithm.

The presence of parasitic modes in the variational midpoint algorithm equation (19) may be demonstrated by performing an eigenvalue analysis. Letting $\mathbf{z} = (\mathbf{x}, u)^T$ and $\vartheta = (\mathbf{A}^\dagger, 0)$, the $h \to 0$ limit of the algorithm is given by:

$$\begin{aligned}&\frac{1}{2}\vartheta_{i,j}\left(\frac{\mathbf{z}_0+\mathbf{z}_1}{2}\right)(z_1^i-z_0^i)+\vartheta_j\left(\frac{\mathbf{z}_0+\mathbf{z}_1}{2}\right)\\&+\frac{1}{2}\vartheta_{i,j}\left(\frac{\mathbf{z}_1+\mathbf{z}_2}{2}\right)(z_2^i-z_1^i)-\vartheta_j\left(\frac{\mathbf{z}_1+\mathbf{z}_2}{2}\right)=0.\end{aligned} \tag{20}$$

In the above, indices range from one to four and we have treated $u_{k+1/2}$ as $(u_k + u_{k+1})/2$ for simplicity and illustration. Linearizing about $\mathbf{z}_0$, we find:

$$\frac{1}{2}(\vartheta_{i,j}(\mathbf{z}_0)-\vartheta_{j,i}(\mathbf{z}_0))(z_2^i-z_0^i)=0. \tag{21}$$

The terms $\vartheta_{i,j} - \vartheta_{j,i}$ are the components of the guiding center symplectic structure Ω defined in equation (11) and therefore form an invertible matrix. The ansatz that $\mathbf{z}_2 = \lambda\ \mathbf{z}_1 = \lambda^2\ \mathbf{z}_0$ yields the eigenvalue equation:

$$(\lambda^2 - 1)\mathbf{z}_0 = 0. \tag{22}$$

For our four dimensional system of interest, this yields four roots at $\lambda = 1$ and four at $\lambda = -1$. The behavior corresponding to the $\lambda = 1$ roots is referred to as the 'principle mode', as it corresponds to a smooth trajectory in the $h \to 0$ limit [1, 20, 21]. The behavior at $\lambda = -1$ is referred to as the 'parasitic mode', as the trajectory oscillates between even- and odd-numbered numerical time steps. Indeed, we see from equation (21) that the trajectory on even-numbered steps is completely decoupled from the trajectory on the odd-numbered steps, for this linearized system.

Performing the same eigenvalue analysis but with u staggered to half-integer steps, i.e. $(u_k + u_{k+1})/2 \to u_{k+1/2}$, demonstrates the stabilizing impact of this staggering. In particular, one finds that one of the parasitic roots is eliminated: four principle roots exist at $\lambda = +1$ and three parasitic roots exist at $\lambda = -1$. This explains the stabilizing impact of staggering the parallel velocity u observed in the original studies of the midpoint guiding center variational integrator [16]. Such a staggering is enabled by the lack of dependence of the guiding center Lagrangian on $\dot{u}$ and cannot be applied to any of the spatial coordinates without transforming the guiding center Lagrangian.

The most important consideration is whether the parasitic modes are stable or unstable. The above linear analysis shows the modes to be marginally stable for the variational midpoint algorithm. Backward error analysis may be performed to derive high-dimensional differential equations governing the parasitic mode behavior [1, 21], but the analysis for nonlinear stability can be complicated. Empirically, we find the modes to be weakly unstable—growing to detrimental amplitudes after several hundred or thousand toroidal transits, if at all, depending on the initial conditions and the electromagnetic field configuration.

Given the weak instability of the parasitic modes, the initial amplitude of the undesired modes is an important factor in determining the overall impact of the oscillations on the numerical fidelity. As might be expected, the initial amplitude of the parasitic modes is determined by the full set of initial conditions; as can be observed from the two-step variational guiding center algorithm, the number of excess initial conditions matches the number of parasitic modes. Careful initialization of the system has a strong impact on the numerical fidelity of the variational guiding center algorithm.

3.2.2. Initial conditions. Typically, initial conditions for multistep methods are generated by accurately approximating the true solution at as many instances in time as needed to begin iterating the update rule. Backward error analysis of the multistep system, however, reveals that this is not an optimal

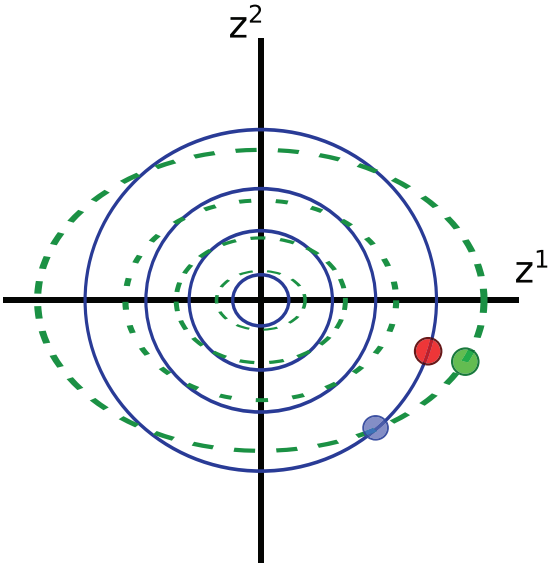

Figure 1. Prototypical phase portrait illustrating the standard starting procedure (red circle) and stabilizing backward error initialization procedure (green circle) based on a common initial condition (blue circle). Blue curves represent the true solution of the equation being modeled, while dashed green curves represent the behavior of the principle mode of the multistep method. The extent to which the second initial condition differs from the green circle is the extent to which parasitic modes will be initialized with non-zero amplitude in the numerical trajectory.

strategy for minimizing parasitic mode behavior [1, 21, 23]. Instead, one should sample initial conditions along the trajectory of the principle component of the multistep algorithm. Doing so requires constructing a differential equation whose solution coincides with the non-parasitic component of the multistep algorithm. After constructing this differential equation (to the desired order of accuracy in numerical step size), one approximates the solution at the initial condition times with an accurate one-step method. Illustration of the backward error starting procedure is provided in figure 1.

The algebra involved in the construction of the backward error differential equation can rapidly grow unwieldy, even though the fundamental operations are basically Taylor expansions. For linear multistep methods, concise representations have been obtained by using rooted tree notation and theorems about b-series [20]. Here, we'll leverage the differential geometry of the variational algorithms and properties of Lie derivatives to maintain concise expressions.

First, we require a precise definition of the backward error differential equation. Backward error analysis seeks to determine a function $\tilde{X}(\mathbf{z})$, called the 'modified vector field', such that solutions to the differential equation $\dot{\mathbf{z}} = \tilde{X}(\mathbf{z})$ satisfy the discrete Euler–Lagrange equations when sampled at time instants represented by the numerical trajectory. Here, $\mathbf{z}$ represents the coordinates of the guiding center system, or more generally, the Hamiltonian phase space. Notationally, the solution of the backward error differential equation is a t-dependent map $\tilde{\varphi}_t$ satisfying the two conditions:

$$\frac{\mathrm{d}\tilde{\varphi}_t}{\mathrm{d}t} = \tilde{X}, \tag{23}$$

and:

$$D_2 L_d(\mathbf{z}_0, \tilde{\varphi}_h(\mathbf{z}_0)) + D_1 L_d(\tilde{\varphi}_h(\mathbf{z}_0), \tilde{\varphi}_{2h}(\mathbf{z}_0)) = 0, \tag{24}$$

where h is the numerical step size used for a particular simulation. The first condition is simply the statement that $\tilde{\varphi}_t$ is the solution of the backward error differential equation (it is the time-t flow map of the modified vector field) and the second condition is the statement that trajectories formed by sampling the solution at h-sized intervals satisfy the discrete Euler–Lagrange equations. The fact that $\tilde{\varphi}_t$ depends only on a single position precludes the possibility of parasitic modes in the solution of the backward error differential equation.

To leverage equation (24) as a constraint for determining the unknown function $\tilde{X}(\mathbf{z})$, one assumes the modified vector field may be represented as a series in the numerical step size h:

$$\tilde{X} = X_0 + hX_1 + h^2 X_2 + \dots, \tag{25}$$

for some functions X_i. The unknown X_i may be iteratively determined by expanding equation (24) about the initial time $t = 0$. It is possible to perform this expansion as a standard Taylor series, but Lie derivatives are better suited for the task. Lie derivatives measure the amount of change in a function (or differential form) in the direction of the solution of a differential equation specified by a vector field—just like that of equation (23). There also exist many useful identities for simplifying expressions with Lie derivatives and differential forms. Letting $\pounds_X$ denote the Lie derivative with respect to the vector field X, the expanding equation (24) about the initial time $t = 0$ yields:

$$\begin{aligned}
&[h^0(d_2 L_d(z_0, z_1) + d_1 L_d(z_1, z_2)) \\
&\quad + h^1\left(\pounds_{(0,\tilde{X})} d_2 L_d(z_0, z_1) + \pounds_{(\tilde{X},2\tilde{X})} d_1 L_d(z_1, z_2)\right) \\
&\quad + h^2\left(\pounds_{(0,\tilde{X})}\pounds_{(0,\tilde{X})} d_2 L_d(z_0, z_1) + \pounds_{(\tilde{X},2\tilde{X})}\pounds_{(\tilde{X},2\tilde{X})} d_1 L_d(z_1, z_2)\right) \\
&\quad + \dots]_{z_2=z_1=z_0} = 0.
\end{aligned} \tag{26}$$

Here, d_i denotes exterior derivative with respect to the i-th argument. To determine X_i, collect the preceding expression in powers of h and set to zero. In general, the h^p term specifies the function $X_{p-1}(\mathbf{z})$ in terms of lower-order X_i functions, the Hamiltonian and derivatives of these quantities. Calculation of these constraints may be automated using a symbolic algebra computational package. For the midpoint discrete Lagrangian defined in equation (18), the h^0 and h^1 terms yield the constraint that the lowest-order function X_0 is equal to $(\dot{\mathbf{x}}, \dot{u})$ in the guiding center equations of motion defined in equation (9). This result is expected for any consistent algorithm. Continuing the procedure to higher order yields constraints determining the functions $X_{i>0}(\mathbf{z})$ and truncating the procedure yields a differential equation that may be used to initialize the guiding center variational integrator.

The parasitic mode amplitude reduction caused by backward error initialization is demonstrated in figure 2. For a simple test case, a guiding center particle is initialized in a straight magnetic field $\mathbf{B} = \hat{\mathbf{z}}$ and quadratic electric potential $\phi = z^2/2$. Initial conditions are sampled first along true solutions to the guiding center equations and secondly along the modified vector field $\tilde{X}$ truncated after determining the

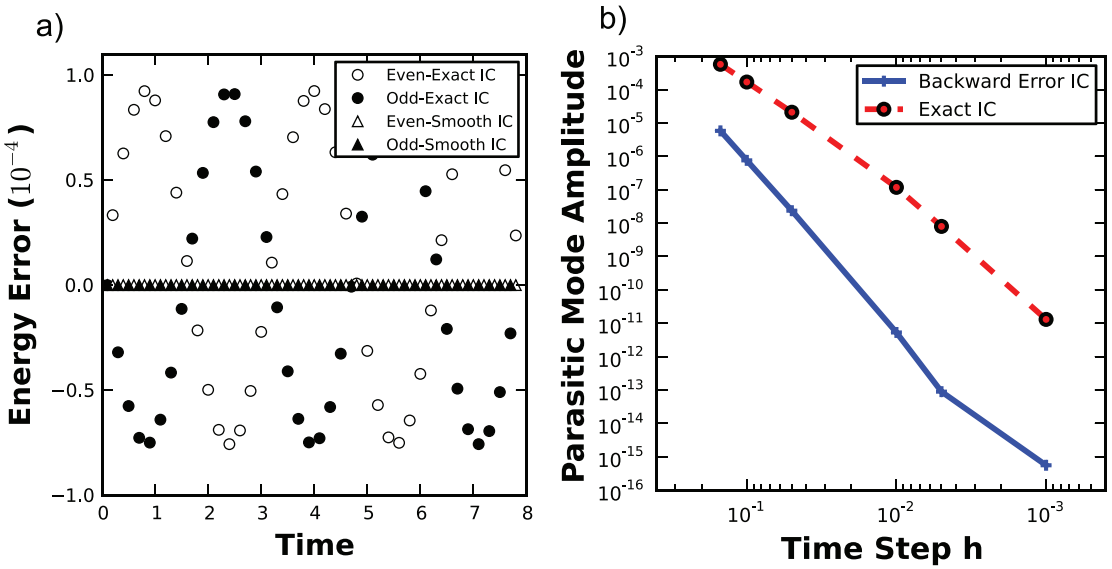

Figure 2. Demonstration of reduced parasitic mode amplitude by backward error initialization. A single non-zero correction term is retained in the modified vector field at order h^2. (*a*) Energy of a guiding center particle in straight magnetic field and quadratic electric potential. The trajectory initialized with the true solution (circles) exhibits a prominent even-odd oscillation in the energy, while the backward error initialized trajectory (triangles) is significantly smoother. (*b*) Scaling of parasitic mode amplitude with true solution initialization and backward error initialization.

non-zero function X_2. The mode-amplitude reduction is directly apparent in the numerical energy and a scan in numerical step size indicates the backward error initialized parasitic mode varies as $\mathcal{O}(h^5)$ while the true-solution initialized parasitic mode scales with $\mathcal{O}(h^3)$. The step size scalings are a consequence of the level of agreement between the differential equation used to generate the initial conditions and the modified vector field of equation (25).

3.2.3. Conservation properties. In addition to stability considerations, the multistep aspect of the variational guiding center algorithms complicates the interpretation of the conserved quantities. As stated at the beginning of the section, the most natural notion of a symplectic guiding center algorithm is a numerical time advance preserving the guiding center symplectic structure. Unfortunately, the multistep dynamics preserve a structure on a larger dimensional space than the physical dynamics. The excellent long-term behavior is then a surprising feature of the variational midpoint algorithm equation (19). To explain the observed long-term numerical fidelity, we demonstrate that the *principle* mode preserves a two-form on the original space. The presence of a preserved structure is an indication that the long-term dynamics will behave well provided the parasitic modes remain small.

First, we analyze the symplectic structure preserved by the multistep variational midpoint algorithm equation (19). Calculation of a preserved two-form is facilitated by the discrete variational principle and has been performed for variational integrators in general in [10] and for the guiding center system in [14, 15, 17]. The calculation proceeds as follows. In contrast to the discrete action of equation (15), which acts on arbitrary discrete trajectories $\{\mathbf{z}_k\}_{k=0}^N$, consider the *restricted* discrete action, $\bar{S}_d$, which acts on discrete paths satisfying the discrete Euler–Lagrange equations:

$$\bar{S}_d(\mathbf{z}_0, \mathbf{z}_1) = \sum_{k=0}^{N} L_d\left(\varphi_{kh}(\mathbf{z}_0, \mathbf{z}_1)\right). \tag{27}$$

Here, $\varphi_h(\mathbf{z}_{k-1}, \mathbf{z}_k) = (\mathbf{z}_k, \mathbf{z}_{k+1})$ according to equation (16). An exterior derivative of the restricted action yields:

$$\mathrm{d}\bar{S}_d(\mathbf{z}_0, \mathbf{z}_1) = d_1 L_d(\mathbf{z}_0, \mathbf{z}_1) + \left(\varphi^*_{(N-1)h} d_2 L_d\right)(\mathbf{z}_0, \mathbf{z}_1), \tag{28}$$

where $\varphi^*_{(N-1)h}$ denotes the pull-back introduced in section 2.1. All other terms in the summation vanish because the discrete trajectory satisfies the discrete Euler–Lagrange equations. An additional exterior derivative together with $d^2 = 0$ obtains the desired result:

$$\varphi^*_{(N-1)h} d_1 d_2 L_d(\mathbf{z}_0, \mathbf{z}_1) = d_1 d_2 L_d(\mathbf{z}_0, \mathbf{z}_1). \tag{29}$$

That is, φ_h is symplectic with discrete symplectic structure Ω_d given in coordinates by:

$$\Omega_d = \frac{\partial^2 L_d}{\partial z_0^i \partial z_1^j} \mathrm{d}z_0^i \wedge \mathrm{d}z_1^j. \tag{30}$$

The discrete symplectic structure Ω_d may be calculated for particular choices of discrete Lagrangian according to equation (30). For the purposes of this discussion, the significant feature of equation (30) is that Ω_d is defined on a space *twice* as large as that on which continuous dynamics occur. Using the notation of section (3.2.1), the continuous guiding center symplectic structure has the form $\Omega = \vartheta_{i,j}\, \mathrm{d}z^i \wedge \mathrm{d}z^j$; it is defined on a four-dimensional space. In contrast, Ω_d is defined on an eight-dimensional space, according to equation (30). This discrepancy explains the possibility of divergent parasitic modes despite constructing a structure-preserving algorithm from

the onset. In particular, the bounded energy error obtained via backward error analysis for symplectic algorithms is not directly applicable to the multistep variational algorithms constructed by discretizing the phase-space action principle used to formulate the non-canonical guiding center dynamics.

Despite the discouraging result of the preceding calculation, the excellent long-term numerical fidelity observed in variational guiding center algorithms suggests that the numerical dynamics behave well when the parasitic modes are not prominent. To analyze the behavior of the non-parasitic component of the guiding center variational algorithms, we again turn to a feature of the numerical analysis literature on multistep algorithms. For the selection of stable initial conditions, we supposed a map $\tilde{\varphi}_h$ that acted directly on the original dynamical space, as defined in equation (24). Indeed, such a map has played an important role in the analysis of multistep methods and is referred to as the 'underlying one-step method' [24]. For the long-term assessment of the principle mode of the variational midpoint algorithm, it is the conservation properties of $\tilde{\varphi}_h$ that are of interest.

The conservation properties of the underlying one-step method $\tilde{\varphi}_h$ are similarly calculated by restricting the discrete action to act on paths generated by the map $\tilde{\varphi}_h$. The procedure does not substantially differ than the multistep calculation and the resulting discrete symplectic structure $\tilde{\Omega}_d$ is given by:

$$\tilde{\Omega}_d = \left(\frac{\partial^2 L_d}{\partial z_0^i \partial z_1^j} \right)_{(\mathbf{z}_0, \mathbf{z}_1) = (\mathbf{z}, \tilde{\varphi}_h(\mathbf{z}))} \left(\tilde{\varphi}_h^j \right)_{,k} \mathrm{d}z^i \wedge \mathrm{d}z^k \,. \tag{31}$$

As an explicit representation of $\tilde{\varphi}_h$ is not known for non-zero h, it is difficult to represent $\tilde{\Omega}_d$ directly in terms of known quantities for the midpoint discrete Lagrangian equation (18). However, in the limit $h \to 0$, $\tilde{\varphi}_0$ is the identity map and $\tilde{\Omega}_d$ reduces to the continuous symplectic structure. Most significantly, the symplectic structure $\tilde{\Omega}_d$ resides on a four-dimensional space even for finite h.

Overall, the symplecticity of the underlying one-step method $\tilde{\varphi}_h$ with respect to $\tilde{\Omega}_d$ is a moderately encouraging result. For nonzero h, the discrete two-form differs from that of the continuous dynamics. However, the principle mode behavior is Hamiltonian, converging to the original Hamiltonian system in the zero step size limit. While the sense in which it is a nearby Hamiltonian system differs from that of conventional symplectic integrator trajectories, the long-term numerical behavior of the variational midpoint algorithm suggests that the preservation of $\tilde{\Omega}_d$ is effective for constraining the numerical dynamics to remain close to the true dynamics.

3.3. Equilibrium interfaces

The final practical consideration for implementing variational guiding center algorithms is the need to extract the magnetic vector potential from experimental equilibria. To begin performing experimentally-relevant calculations, we have interfaced the guiding center variational algorithms with the EFIT equilibrium code [25]. The ability to model test particles in experimentally determined equilibria is an important progression from previous studies in which the fields were analytically prescribed by a known vector potential and axisymmetry was used to reduce the dimensionality of the system [14, 15, 17]. Although EFIT produces axisymmetric equilibria, we perform the calculation in three spatial dimensions to allow for future addition of three-dimensional magnetic perturbations. The incremental difficulty in calculating particle trajectories that model experimental observations is the requirement of interpolating magnetic geometry specified at discrete locations on a numerical grid.

In the case of EFIT, the magnetic geometry of an experimental tokamak discharge is represented by the poloidal flux ψ on a two-dimensional spatial grid and a poloidal current function F on a flux grid. That is, EFIT specifies $\psi(R_i, z_j)$ and $F(\psi_i)$, where (R, z, θ) are cylindrical coordinates and indices (i, j) now identify points on the numerical grid. From these quantities, the magnetic field may be determined according to:

$$\mathbf{B} = \frac{1}{R} \left((-\psi_{,z})\, \hat{\mathbf{r}} + F\, \hat{\boldsymbol{\theta}} + \psi_{,R}\, \hat{\mathbf{z}} \right). \tag{32}$$

For evaluation of the magnetic field at arbitrary position, one must interpolate $F(\psi\ (R,\ z))$ and $\nabla\psi(R,\ z)$ to the location of interest.

To model the guiding center equations of motion with the variational midpoint algorithm equation (19), a magnetic vector potential $\mathbf{A}$ must be constructed such that $\nabla \times \mathbf{A}$ yields the EFIT magnetic configuration in equation (32). As in [26], we determine a vector potential by selecting an electromagnetic gauge and integrating the magnetic field the determine the unknown functions. Specifically, suppose a vector potential of the form:

$$\mathbf{A} = \psi\, \nabla\theta + A_z\, \nabla z \,. \tag{33}$$

The magnetic field is calculated according to:

$$\mathbf{B} = \nabla\mathbf{A} = \psi_{,R}\, \nabla R \times \nabla\theta + \psi_{,z}\, \nabla z \times \nabla\theta + A_{z,R}\, \nabla R \times \nabla z \,. \tag{34}$$

Accounting for the metric tensor and matching components, the vector potential yields the magnetic field of equation (32) if:

$$A_{z,R} = -\frac{F}{R} \,. \tag{35}$$

Construction of the magnetic vector potential then consists of the following steps: First, represent $\psi(R, z)$ using local bicubic polynomials. Second, evaluate $F(\psi\ (R_i,\ z_j))$ on the grid and represent the function F/R using local bicubic polynomials. Third, integrate to determine $A_z(R, z) = \int_0^R \frac{F}{R'} \mathrm{d}R'$. The vector potential can then be interpolated to any location in the domain for evaluation in the variational midpoint algorithm. The additional magnetic field quantities are derived from the interpolating polynomial of the vector potential.

4. Results

Now that the context, formal properties and practical considerations of the variational guiding center algorithms have been established, we turn to the numerical results. This section presents the variational algorithm's performance in analytic and

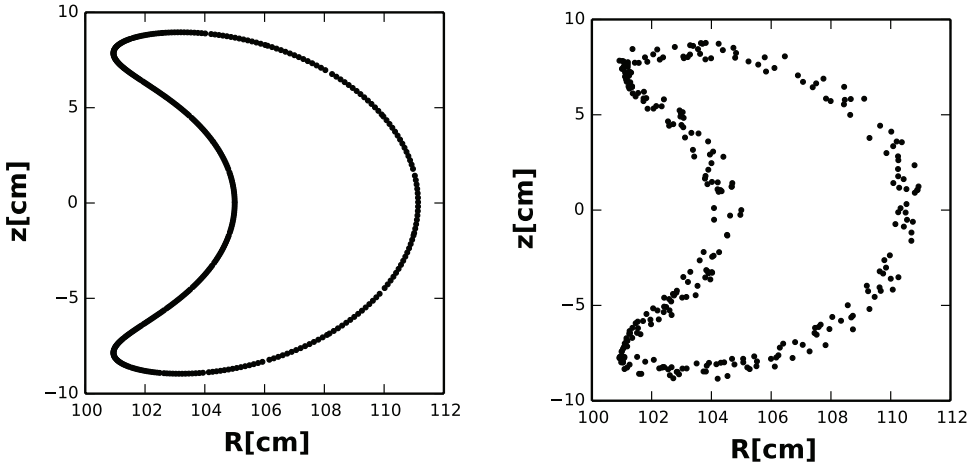

Figure 3. Comparison of the second-order variational midpoint algorithm (left) and fourth-order Runge–Kutta (right) for the integration of a trapped particle trajectory. Particle is a 2 keV ion with initial state $(R, \theta, z, u) = (1.05\text{ m}, 0\text{ rad}, 0\text{ m}, 1.3 \times 10^5\text{ m s}^{-1})$. Numerical step size is $h = 12\ \mu$s for both tests and total simulated time is 3.6 s.

experimental equilibria and shows time to solution improvements for large numbers of particles using GPGPU hardware.

4.1. Analytic axisymmetric tokamak

As an initial test case, we consider a simple analytic toroidal geometry given by:

$$\mathbf{A} = \frac{B_0 R_0 z}{2R}\mathbf{d}R + \frac{B_0 r^2}{2q}\mathbf{d}\theta - \log\left(\frac{R}{R_0}\right)\frac{B_0 R_0}{2}\mathbf{d}z, \qquad (36)$$

where B_0, R_0 are constants, q is the safety factor and $r = \sqrt{z^2 + (R - R_0)^2}$ the minor radius. This field was used for the test case in [15], but the present study differs in the choice of discrete Lagrangian and by tracking the full four-dimensional motion in (R, θ, z, u).

The results of a trapped particle with $B_0 = 1$ T, $R_0 = 1$ m and $q = \sqrt{2}$ are shown in figure 3. Characteristically, the conservative variational algorithm out-performs the non-conservative Runge–Kutta method over long simulation times. The orbit of the 2 keV ion artificially degrades when using the Runge–Kutta algorithm, despite the higher-order local accuracy of the method. This degradation of numerical fidelity manifests both in the orbit topology and in scalar quantities like the energy; interestingly, the orbit topology noticeably deteriorates on a shorter timescale than the energy. In this test case, the closed orbit of the variational integrator interweaves the original constant energy surface with a fractional energy error amplitude of 1×10^{-3}. Meanwhile, the Runge–Kutta method accumulates energy error without bound, but does so very slowly: a total of 7×10^{-4} fractional energy error has accumulated over the run shown in figure 3. Essentially, energy conservation is only a single constraint on the four dimensional guiding center $(\mathbf{x}, u)$ space and does not reflect the visually-apparent degradation of the spatial orbit topology.

4.2. Experimental tokamak equilibria

To demonstrate practical relevance of the variational guiding center algorithms, the guiding center test particle code has been interfaced with the EFIT magnetic equilibrium code. While interpolated magnetic fields do not formally differ from concise global analytic expressions, several practical considerations arise as detailed in section 3.3.

For a test case, we have simulated a 10 keV ion in an experimentally determined equilibrium from the National Spherical Tokamak Experiment (NSTX). Shown in figure 4 is a sample trapped particle trajectory and convergence test in numerical step size. The spatial trajectory remains tighter for the variational algorithm than the Runge–Kutta algorithm of same order. Convergence of the variational algorithm to an accurate short-time simulation demonstrates successful construction of the magnetic vector potential necessary for equation (19).

It is interesting to note that the test particles drift in the EFIT magnetic geometry represented using local bicubic polynomials. As the numerical step size decreases, the trajectories increasingly approximate closed orbits. However, the local error of the algorithm allows particles to sample magnetic geometry away from their trajectory, resulting in an overall drift. This is likely a result of the discontinuity of the second derivatives of the bicubic polynomials. Because $\mathbf{A}$ is interpolated with cubic polynomials, the ∇B terms appearing in the guiding center equations of motion exhibit discontinuities at cell boundaries. Smoother interpolants such as bicubic splines may therefore eliminate the drifts observed in the experimental magnetic geometry. Precedence exists for requiring smooth interpolation functions when performing guiding center calculations [9].

4.3. GPGPU parallelization

In conjunction with algorithmic advances, innovations in computational hardware may be leveraged to improve guiding center test particle calculations. Given the increasing prevalence of GPGPU hardware at high performance computing facilities, parallelizing test particle codes to utilize such hardware can significantly reduce the run time for a given problem. The lack of interaction among drifting test particles simplifies the difficulty of parallelization and motivates the investment of time to use highly parallel resources.

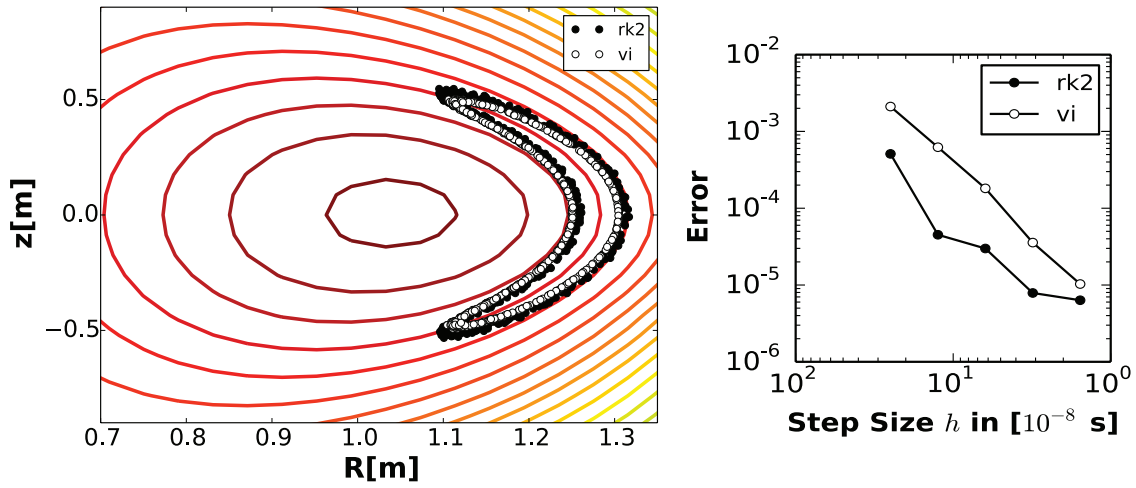

Figure 4. Sample trapped particle trajectory of a 10 keV ion in an NSTX EFIT equilibrium over 1100 bounce times with numerical step size $h = 1.0 \times 10^{-7}$ s **Left)** Overlay of second-order Runge–Kutta (black) and second-order variational midpoint guiding center algorithms (white). **Right)** Convergence of variational midpoint trajectory to an accurate trajectory generated using fourth-order Runge–Kutta with step size $h = 1.0 \times 10^{-9}$ s.

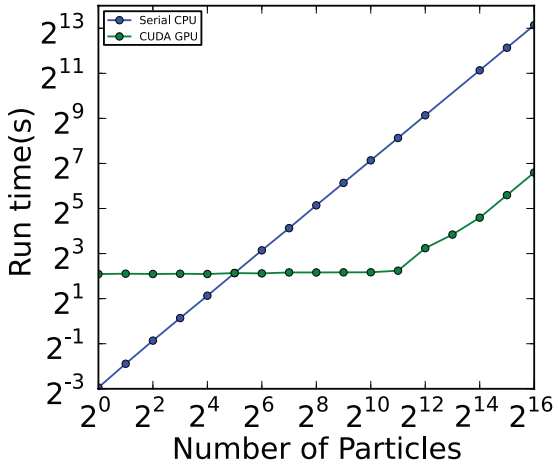

Figure 5. Run time in seconds as a function of number of particles for a single core 2.5 GHz AMD Opteron CPU **(blue)** and a 2496 core nVidia Tesla k20m card **(green)**. The GPGPU run time only increases noticeably once the number of particles exceeds the number of GPGPU cores.

Using the CUDA programming language, we have implemented a parallel driver for the guiding center test particle code. The run time as a function of the number of particles is shown in figure 5, where comparison is made between using the serial driver on a single 2.5 GHz CPU core and the CUDA driver on a 2496 core nVidia Tesla k20m GPGPU. For small numbers of particles, the CPU is faster by a factor of approximately 16. As the number of particles increases, the GPGPU becomes the more efficient hardware for the task, exhibiting negligible increase in run time until the number of particles exceeds the number of GPGPU cores. For large numbers of particles, the GPGPU is approximately 100 times faster than the single core CPU.

The strong performance of the GPGPU should be considered within the broader perspective of computing hardware. Nearly all CPU computing nodes possess more than a single core for use and CPU parallelizttion tools including MPI and OpenMP can leverage this hardware. A more insightful comparison between the CPU and GPGPU hardware would compare the run time of a 16 core CPU to that of the GPGPU device. Extrapolating the preceding results, we would find use of the GPGPU device remains advantageous over 16 CPU cores, exhibiting a time to solution improvement factor of approximately six for large numbers of guiding center test particles.

5. Conclusion

In summary, variational algorithms exhibit strong potential for guiding center test particle calculations due to their achievable long-term fidelity and parallelizability. Unique challenges emerge in the guiding center context, resulting from the non-canonical Hamiltonian description. Discretization of the degenerate guiding center Lagrangian results in a somewhat atypical variational integrator: the variational algorithm constitutes a multistep method for advancing the guiding center equations of motion. Consequences of the multistep algorithm include the presence of unphysical parasitic mode oscillations, which can be mitigated using a backward error initialization procedure. While the multistep map preserves a symplectic structure on a larger space than the physical guiding center system, the underlying one-step method preserves a structure on the original phase space, leading to excellent long-term numerical fidelity whenever the parasitic components remain small. This desirable long-term behavior has been demonstrated in simple, analytic axisymmetric equilibria as well as fields interpolated from experimental equilibrium reconstructions. To interface with the EFIT equilibrium code, a magnetic vector potential was constructed by integrating the Θ-component of the magnetic field in the radial direction. Run time was reduced for large numbers of test particles by parallelizing the calculation using the CUDA programming language. Combined, this contribution establishes context for understanding variational guiding center algorithms, identifies unique challenges and mitigation strategies that arise when employing these methods and demonstrates the viability

of these techniques for performing experimentally-relevant calculations.

Stepping back, the most significant drawback of the variational guiding center algorithms is the presence of parasitic mode oscillations. Whereas the increased run time due to the implicit nature of the algorithm can be mitigated with faster nonlinear solves and parallel implementation, stability of a long-term algorithm is critical for widespread adoption of the method. The proposed initialization strategy delays the onset of marginally-stable parasitic modes—often for sufficiently long times—but the pursuit of more robust mitigation strategies is both prudent and underway. One tactic is to survey the distinct families of discretization strategies for constructing variational integrators [11–13]. It seems improbable that the simple midpoint discretization employed in this article is the most stable of all possible methods and an empirical testing of several classes of algorithms could identify methods with superior parasitic mode stability. More systematically, a re-formulation of the variational integrator methodology suited for the phase-space Lagrangian construction may avoid the multi-step nature altogether. For canonical phase-space Lagrangians, different classes of generating functions are better suited for the discretization and directly lead to one-step symplectic methods [27, 28]. A generalization of this methodology to non-canonical phase-space Lagrangians could achieve the desired non-canonically symplectic one-step methods.

Looking forward, an important next step in the context of guiding center test particle dynamics is to incorporate collisional effects in the conservative numerical algorithms. While fast particles such as fusion alphas and runaway electrons may be approximated as collisionless over short time scales, collisions inevitably play an important role over longer time scales. For non-dissipative stochastic effects, such as a pitch-angle scattering event, it is likely the system may be formulated as a stochastic Hamiltonian system [29, 30] enabling the construction of stochastic variational integrators by discretizing the corresponding action principle [31, 32]. For dissipative effects, including polarization drag, the non-Hamiltonian dynamics may still be formulated (and discretized) as an action extremization condition by using a Lagrange-d'Alembert variational principle [10]. The potential benefits of such constructions for the time evolution of fusion-relevant fast particle distributions are an exciting prospect.

Overall, variational integration is a promising approach to performing high-fidelity guiding center test particle calculations for the present and upcoming generation of magnetically-confined plasmas. It is our hope that further development of the formal conservation properties and high-performance computing capabilities of these methods will result in their widespread use for ITER-relevant calculations.

Acknowledgments

The authors are grateful to J W Burby and M Kraus for helpful discussions on Hamiltonian systems and variational integrators. Similarly, we would like to thank N Logan and S Hudson for assistance with the EFIT equilibrium code. This work was performed under US Department of Energy contract DE-AC02-09CH11466.

References

[1] Hairer E, Lubich C and Wanner G 2006 *Geometric Numerical Integration* (New York: Springer)
[2] Littlejohn R G 1983 Variational principles of guiding centre motion *J. Plasma Phys.* **29** 111–25
[3] Cary J R and Brizard A J 2009 Hamiltonian theory of guiding-center motion *Rev. Mod. Phys.* **81** 693
[4] Abraham R and Marsden J E 1987 *Foundations of Mechanics* (Reading, MA: Addison-Wesley)
[5] Marsden J E and Ratiu T S 1999 *Introduction to Mechanics and Symmetry* (New York: Springer)
[6] Karasözen B 2004 Poisson integrators *Math. Comput. Modelling* **40** 1225–44
[7] White R B and Chance M S 1984 Hamiltonian guiding center drift orbit calculation for plasmas of arbitrary cross section *Phys. Fluids* **27** 2455
[8] White R and Zakharov L E 2003 Hamiltonian guiding center equations in toroidal magnetic configurations *Phys. Plasmas* **10** 573
[9] Pfefferlé D, Graves J P, Cooper W A, Misev C, Chapman I T and Turnyanskly ans M 2014 NBI fast ion confinement in the helical core of MAST hybrid-like plasmas *Nucl. Fusion* **54** 064020
[10] Marsden J E and West M 2001 Discrete mechanics and variational integrators *Acta Numer.* **10** 1–5
[11] Leok M and Shingel T 2011 Prolongation-collocation variational integrators *IMA J. Numer. Anal.* **32** 1194–216
[12] Leok M and Shingel T 2012 General techniques for constructing variational integrators *Front. Math. China* **7** 273–303
[13] Hall J and Leok M 2014 Spectral variational integrators *Numerische Mathematik* doi:10.1007/s00211-014-0679-0
[14] Qin H and Guan X 2008 Variational symplectic integrator for long-time simulations of the guiding-center motion of charged particles in general magnetic fields *Phys. Rev. Lett.* **100** 035006
[15] Qin H, Guan X and Tang W M 2009 Variational symplectic algorithm for guiding center dynamics and its application in tokamak geometry *Phys. Plasmas* **16** 042510
[16] Li J, Qin H, Pu Z, Xie L and Fu S 2011 Variational symplectic algorithm for guiding center dynamics in the inner magnetosphere *Phys. Plasmas* **18** 052902
[17] Squire J, Qin H and Tang W M 2012 Gauge properties of the guiding center variational symplectic integrator *Phys. Plasmas* **19** 052501
[18] Kraus M 2013 Variational integrators in plasma physics *PhD Thesis* Technische Universität, Munchen
[19] Arnold V I 1989 *Mathematical Methods of Classical Mechanics* (New York: Springer)
[20] Hairer E 1999 Backward error analysis for multistep methods *Numer. Math.* **84** 199–232
[21] Hairer E and Lubich C 2004 Symmetric multistep methods over long times *Numer. Math.* **97** 699–723
[22] Tang Y-F 1993 The symplecticity of multi-step methods *Comput. Math. Appl.* **25** 83–90
[23] D'Ambrosio R and Hairer E 2014 Long-term stability of multi-value methods for ordinary differential equations *J. Sci. Comput.* **60** 627–40
[24] Kirchgraber U 1986 Multi-step methods are essentially one-step methods *Numer. Meth.* **48** 85–90
[25] Lao L L, John H S, Stambaugh R D and Pfeiffer W 1985 Separation of $\bar{\beta}_p$ and l_i in tokamaks of non-circular cross-section *Nucl. Fusion* **25** 1421

[26] Finn J M and Chacón L 2005 Volume preserving integrators for solenoidal fields on a grid *Phys. Plasmas* **12** 054503
[27] Lall S and West M 2006 Discrete variational hamiltonian mechanics *J. Phys.* A **39** 5509–19
[28] Leok M and Zhang J 2011 Discrete hamiltonian variational integrators *IMA J. Numer. Anal.* **31** 1497–532
[29] Lázaro -Camí J-A and Ortega J-P 2008 Stochastic hamiltonian dynamical systems *Rep. Math. Phys.* **61** 65–122
[30] Burby J W and Qin H 2013 Hamiltonian mechanics of stochastic acceleration *Phys. Rev. Lett.* **111** 195001
[31] Bou-Rabee N and Owhadi H 2008 Stochastic variational integrators *IMA J. Numer. Anal.* **29** 421
[32] Bou-Rabee N and Owhadi H 2010 Long-run accuracy of variational integrators in the stochastic context *SIAM J. Numer. Anal.* **48** 278–97